Magnetic Resonance Imaging 34 (2016) 473–482

Contents lists available at ScienceDirect

Magnetic Resonance Imaging

journal homepage: www.mrijournal.com

Original contribution

Real time dynamic MRI by exploiting spatial and temporal sparsity

Chen Chen [a], Yeqing Li [a], Leon Axel [b], Junzhou Huang [a,*]

[a] Department of Computer Science and Engineering University of Texas at Arlington, Arlington, TX, 76019
[b] Department of Radiology, New York University, New York, NY, 10016

ARTICLE INFO

Article history:
Received 31 August 2015
Accepted 26 October 2015

Keywords:
Sparse MRI
Compressed sensing MRI
Total variation
Reweighted least squares algorithm

ABSTRACT

Online imaging requires that the reconstruction of current frame only depends on the previous frames, and real time imaging is the desired case. In this work, we propose a novel scheme for real time dynamic magnetic resonance imaging (dMRI) reconstruction. Different from previous methods, the reconstructions of the second frame to the last frame are independent in our scheme, which only require the first frame as the reference image. Therefore, this scheme can be naturally implemented in parallel. After the first frame is reconstructed, all the later frames can be processed as soon as the k-space data are acquired. As an extension of the conventional spatial total variation, a new online model called dynamic total variation is used to exploit the sparsity on both spatial and temporal domains in dMRI. In real time dMRI, each frame is required to be reconstructed very fast. We then design a novel reweighted least squares algorithm to solve the challenging problem. Motivated by the special structure of partial Fourier transform in sparse MRI, this algorithm is accelerated by the preconditioned conjugate gradient descent method. The proposed method is compared with 4 state-of-the-art online and offline methods on two *in-vivo* cardiac dMRI datasets. The experimental results show that our method significantly outperforms previous online methods, and is comparable to the offline methods in terms of reconstruction accuracy.

1. Introduction

Dynamic magnetic resonance imaging (dMRI) is an important medical imaging technique that is widely used in hospitals for medical diagnosis and medical research. In general, there is a trade-off between the spatial resolution and temporal resolution, due to the limitation of acquisition speed of MR scanner. To reduce the scanning time, partial k-space data are acquired for reconstruction instead of full sampling. However, such undersampling often results in aliasing artifacts if the inverse Fourier transform is directly applied. Fortunately, the MR image sequence often provides redundant information in both spatial and temporal domains, which makes the use of compressive sensing (CS) theory [1,2], repeatedly successful in MRI [3–9].

Based on the reconstruction schemes, the dMRI reconstruction methods can be online or offline. Most of existing CS-based methods are offline as they require the data of all frames to be collected before reconstruction. These methods applies sophisticated techniques to exploit the redundancies of the whole dataset, such as motion correction [10–12] dictionary learning [13–16] group clustering [17,18] and low rank approximation [19]. By these offline methods, the MR images can be reconstructed accurately but the drawbacks are their relatively slower speeds and their complex system setup. People may be required to tune multiple system parameters for different data.

Online reconstruction means that the reconstruction of one frame only relies on the previous frames but not the later frames. Therefore, it is possible to reconstruct each frame once the corresponding k-space data are acquired. Of course, online reconstruction is much more challenging due to the lack of entire information as well as the concerns of reconstruction speed. Previous online methods usually assume that the difference between two adjacent frames is very small, either in the intensity or wavelet domain [20–24]. The difference can be reconstructed by sparsity regularization and the images are then updated by these changes. However, due to the lack of entire information, these methods have been shown to be less accurate than the state-of-the-art offline methods. Since the reconstruction of current frame is based on the previous frame, the reconstruction error will be accumulated. Such error accumulation makes these methods not feasible for relatively long sequences. Moreover, it is difficult for these methods to achieve real time reconstruction (i.e. the ideal case of online reconstruction), as they have to wait for the reconstruction of previous frame.

The data acquisition speed has been very fast with some recent developed techniques [25,26] e.g. 20 ms. Due to the concerns of reconstruction speeds, the redundancies in both spatial and temporal domains are often not fully utilized in these works. Hence, reconstruction noise and visible artifacts may be contained in the results. On the other

* Corresponding author.
E-mail address: jzhuang@uta.edu (J. Huang).

http://dx.doi.org/10.1016/j.mri.2015.10.033
0730-725X/

hand, the speeds of CS-based methods are still limited by their intrinsic schemes, although higher accuracy can be achieved.

To bridge this gap, we propose a new online reconstruction scheme, where the first frame is used to guide all the later reconstructions to exploit the temporal redundancy. A comparison with previous online methods is shown in Fig. 1. In contrast to previous serial system, our scheme is parallel and can naturally avoid error accumulation. After the first frame is reconstructed, all the later frames can be processed as soon as the data are acquired.

In this new scheme, the sparsity assumptions in previous online methods may not hold any more. To address this issue, we introduce a new sparsity model called dynamic total variation (dTV), to exploit the sparsity in both spatial and temporal domains. An accelerated reweighted least squares algorithm is proposed to solve the dTV reconstruction by observing the diagonally dominant prior knowledge in CS-MRI (see Section 4 for more details). Finally, the proposed method is validated on *in-vivo* cardiac MR sequences with comparisons to the state-of-the-art online and offline methods. Experimental results show that the dTV is much more effective than the conventional TV on dMRI reconstruction. More importantly, our method achieves comparable accuracy to the state-of-the-art offline methods and significantly outperforms the recent online methods. Our contributions are from the novel scheme, the robust modeling to the efficient algorithm, which make real time dMRI much more feasible than before. Some preliminary results of this work have been presented in MICCAI 2014 [27].

The rest of this paper is organized as follows. In Section 2, we give a brief review of the widely used sparsity models in dMRI. The motivation of this work is explained in Section 3 and the dTV is introduced there. We propose an efficient algorithm to solve the dTV reconstruction problem in Section 4, with step-by-step derivations in details. In Section 5, the proposed method is evaluated on two *in-vivo* cardiac datasets with comparisons to the state-of-the art methods. Finally, we give the conclusion in Section 6.

2. Notations and related work

We denote the image of frame t as x_t and $X = [x_1, x_2, \ldots, x_T]$ denotes the whole T images. Each frame has N pixels. The dMRI reconstruction is to solve x_t from an inverse problem $b_t = R_t F x_t$, where b_t is the measurement vector of frame t which may contain noise; R_t consist M rows of an N-by-N identity matrix; F denotes the Fourier transform. This problem is ill-posed and requires regularization. With the emerging of CS, many methods are proposed to exploit the spatial and temporal sparsity in dMRI reconstruction. It can be formulated as:

$$\min \Phi(X) \ \text{ s.t. } \sum_{t=1}^{T} \|R_t F x_t - b_t\|_2^2 \le \varepsilon, \tag{1}$$

where Φ denotes some sparsity inducing term. Here we review some of the widely used approaches in dMRI.

- *Temporal Fourier transform*. Lustig et al. use the temporal Fourier transform to sparsify periodic motions [4]. That is $\Phi(X) = \|F_t X\|_1$, where F_t denotes the Fourier transform along the temporal direction, $\|\cdot\|_1$ denotes the vector ℓ_1 norm. The wavelet transform is additionally used to sparsify data in the spatial directions. This temporal Fourier transform has been used in many later works, e.g. [12,28].
- *Low rank approximation*. Due to the high correlation among different frames, it is assumed that the matrix X is rank deficient. Therefore, minimizing $\Phi(X) = \|X\|_*$ is used to achieve a rank deficient solution [19,29] where $\|\cdot\|_*$ denotes the nuclear norm of a matrix.
- *Temporal total variation*. The temporal TV assumes that the images changes smoothly along the temporal direction [14,30]. Therefore the gradient along the temporal direction should be small: $\Phi(X) = \|\nabla_t X\|_1$.
- *3D total variation*. The 3D TV is used for regularization in [31], i.e. $\Phi(X) = \sum_i \sqrt{(\nabla_x X)_i^2 + (\nabla_y X)_i^2 + (\nabla_t X)_i^2}$ where i denotes the gradient at the i-th pixel. It is assumed that the MR images are piecewise smooth in all directions.
- *Difference image*. It is widely assumed that the difference image between the current frame and the previous frame should be sparse [12,21,32,33] that is, $\Phi(X) = \|\Delta x\|_1 = \|x_t - x_{t-1}\|_1$. However, this approach is sensitive to motion. This idea has been used in other online reconstruction methods, with the combination of wavelet transform [22] and Kalman filter [20,34]. Asif et al. propose to initialize the reconstruction by standard CS [35]. Then the forward and backward motions are estimated to

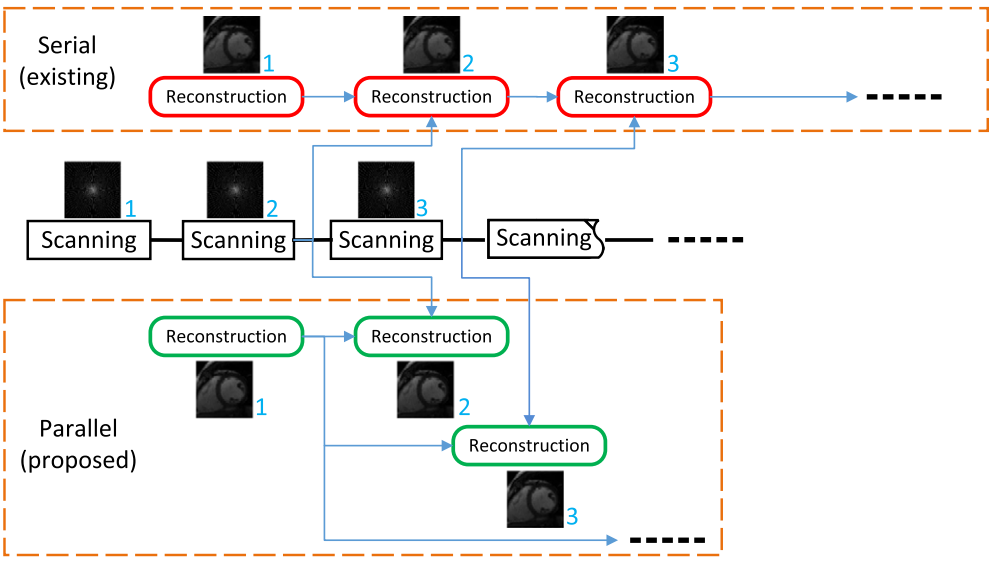

Fig. 1. Comparison between the proposed scheme and the existing online scheme.

Table 1
Comparison of different spatial and temporal methods.

Methods	Spatial	Temporal	Online
Spatial wavelet	✓		✓
Spatial TV	✓		✓
Temporal Fourier		✓	
Low rank		✓	
Temporal TV		✓	
3D TV	✓	✓	
Difference image		✓	✓
dTV	✓	✓	✓

improve the reconstruction. Let E_t and B_t denote the forward and backward motion operator, respectively. The motion correction can be written as $\Phi(X) = \|E_{t-1}x_{t-1} - x_t\|_1 + \|B_{t+1}x_{t+1} - x_t\|_1$. After the correction, the difference image would be sparser.

The comparison of these widely used methods is listed in Table 1. Only our method can exploit both spatial and temporal prior information in the online scheme. We are unable to summarize all the existing methods for dMRI here. Interested readers would refer to Ref. [36] for a more completed survey. Except Refs. [21,22,20] almost all these methods mentioned require the data of all frames to be available and they can only perform offline reconstruction. The existing online methods [21,22,20] are all sequential, where the reconstruction of current frame depends on the previous one. As a result, the reconstruction error will accumulate to the later frames. The experimental results in Ref. [21] demonstrate that the accuracies of these methods are obviously lower than those of the state-of-the-art offline methods.

3. Modeling with dynamic total variation

Dynamic MR images are very similar in the temporal domain, where the same tissues are contained through the whole image sequence. After the first frame is obtained, intuition tells us that the later frames should be very close to it. This motivates us to design the new online reconstruction scheme, which has been presented in Fig. 1. With the prior information in the first frame, it is possible to guide the later reconstructions with fewer k-space measurements. As we always use the first frame but not the previous frame as the reference, the reconstruction problem becomes more challenging. The assumptions in previous online method may not hold any more, e.g. the difference image is sparse [21].

To address this problem, we introduce a new sparsity inducing norm called dynamic total variation (dTV) to utilize both spatial and temporal correlations for online reconstruction. For an image x with N pixels, the dTV is defined as:

$$dTV(x,r) = \sum_{i=1}^{N} \sqrt{(\nabla_x(x-r)_i)^2 + \left(\nabla_y(x-r)\right)^2}, \tag{2}$$

where r denotes a reference image that has similar boundaries as x, ∇_x and ∇_y denote the gradients along the x and y directions. It means that the sparsity in gradient domain is not fixed but dynamic to a reference image. When there is no reference image, i.e. r is a zero image, it is identical to the conventional spatial TV. In this study, we use the first frame as the reference image. In practice, the reference image can be a pre-scanned image with high quality. A similar approach constrained with a reference image has been used in computed tomography (CT) image reconstruction [37].

Compared with the conventional spatial TV and temporal TV, dTV can exploit the sparsity in both temporal and spatial domains simultaneously; compared with 3D TV, dTV is available for online reconstruction.

Therefore, the dMRI reconstruction is formulated as:

$$\min_{x_t} dTV(x_t, x_1), \quad \text{s.t. } \|R_t F x_t - b_t\|_2 \le \varepsilon, \quad t = 2, \ldots, T. \tag{3}$$

Same as that in existing online methods [20–22] the first frame should be reconstructed accurately with more k-space sampling. From this formulation, our scheme can be clearly observed. The reconstruction of each frame (except the first frame) only depends on the first one, but not the previous one. Therefore, it can be implemented in parallel to avoid waiting in the serial scheme.

In this study, we only consider breath-hold imaging. We have a mild assumption, that the motions of organs are bounded (otherwise, the organs will move out of the scanning area). This assumption is quite natural because the cardiac motion is near periodic in breath-hold imaging. If we divide the cardiac motion into several phases, the frame with the closest phase to the first frame should have minimum reconstruction error, and vice versa. Example frames of a cardiac cine dataset are shown in Fig. 2. The difference image between the second frame and the first frame is very sparse, while the difference images at $t = 5$ and $t = 10$ are much less sparse due to the phase mismatch. After a full cardiac circle, the difference image will become very sparse again, e.g. at $t = 20$. One of the advantages of the dTV is that it can always sparsify the images even in the worst case (shown in the second row in Fig. 2). Therefore, the reconstruction accuracy can be improved. It is important to note that we do not require the pixel values to be similar as that assumed in previous online methods, e.g. Ref. [21]. If there are two images with different pixel values but similar tissue boundaries, the difference image in the gradient domain should be still very sparse.

There are two simple ways to extend our method to parallel imaging. When the coil sensitivities are available, it can be combined with SENSE [38] in the k-t SPARSE-SENSE framework [28]:

$$\begin{aligned} &\min_{x_t} dTV(x_t, x_1), \\ &\text{s.t. } \|R_t F E x_t - B_t\|_2 \le \varepsilon, \quad t = 2, \ldots, T. \end{aligned} \tag{4}$$

where $B_t = \begin{bmatrix} b_{1,1} \\ \ldots \\ b_{1,C} \end{bmatrix}$ represents the measurements of different coils; $E = \begin{bmatrix} E_1 \\ \ldots \\ E_C \end{bmatrix}$ denotes the coil sensitivities; C denotes the total number of coils.

When the coil sensitivities are not available, this method can be seamlessly combined with the calibrationless parallel MRI reconstruction [39], by considering the joint gradient sparsity of the images across multiple receiver coils:

$$\begin{aligned} &\min_{x_{t,c}} \sum_{i=1}^{N} \sqrt{\sum_{c=1}^{C} \left(\nabla_x\left(x_{t,c} - x_{1,c}\right)_i\right)^2 + \left(\nabla_y\left(x_{t,c} - x_{1,c}\right)_i\right)^2}, \\ &\text{s.t. } \left\|R_{t,c} F x_{t,c} - b_{t,c}\right\|_2 \le \varepsilon, \quad t = 2, \ldots, T. \end{aligned} \tag{5}$$

where c is the coil index. After the aliased image of each coil is reconstructed, the final field of view can be obtained by the sum-of-squares approach. The coil sensitivity information is not necessary to be estimated in the second approach.

4. Preconditioning for fast MRI reconstruction

The reconstruction speeds of offline methods are often not of big concern. However, fast reconstruction is essential to online methods. In this section, we proposed a new algorithm to efficiently minimize (3). Let $z = x_t - x_1$, and the problem (3) can be written as the Lagrange relaxed form of TV minimization:

$$\min_z \left\{ \frac{1}{2}\|Az - y\|_2^2 + \lambda \|z\|_{TV} \right\}, \tag{6}$$

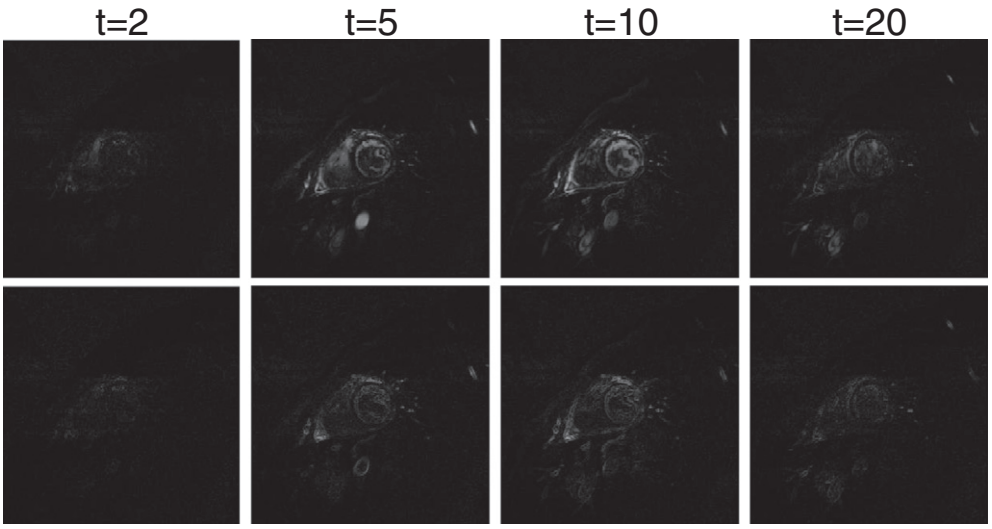

Fig. 2. First row: the difference images between the first frame and the 2nd, 5th, 10th 20th frames for the cardiac cine dataset. Second row: their corresponding gradients.

where $A = R_t F, y = b_t - R_t F x_1$ and λ is a parameter. There are many methods to solve (6) in the literature of convex optimization. Some of them have very fast convergence rate (e.g. [40]), but the computational cost in each iteration is very high. Some other methods are less computationally expensive in each iteration, such as that in Refs. [41,42] while they converge relatively slower. We expect to design an algorithm with both fast convergence and low computational cost.

Our algorithm is based on the reweighted least squares framework [40,43] which can converge exponentially fast [44]. Let D_1, D_2 be two N-by-N two first-order finite difference matrices in vertical and horizontal directions. The TV can be re-formulated as

$$\min_z \left\{ F(z) = \frac{1}{2}\|Az-y\|_2^2 + \lambda \|[D_1 z, D_2 z]\|_{2,1} \right\}, \tag{7}$$

where the $\ell_{2,1}$ norm is the summation of the ℓ_2 norm of each row. Here and later, [,] denotes concatenating the matrices horizontally.

Consider the Young's inequality holding for a general function $g(\cdot) : \mathbb{R} \mapsto \mathbb{R}$:

$$\sqrt{g(x_1)} \le \frac{\sqrt{g(x_2)}}{2} + \frac{g(x_1)}{2\sqrt{g(x_2)}}, \tag{8}$$

with $g(x_2) > 0$ and $g(x_1) \ge 0$. The equality holds only when $g(x_1) = g(x_2)$. Based on this, we majorize (7) by majorization minimization (MM) framework [45]:

$$\begin{aligned} Q\left(z, W^k\right) = {} & \frac{1}{2}\|Az-y\|_2^2 + \frac{\lambda}{2} z^* D_1^* W^k D_1 z \\ & + \frac{\lambda}{2} z^* D_2^* W^k D_2 z + \frac{\lambda}{2} \mathrm{Tr}\left(\left(W^k\right)^{-1}\right), \end{aligned} \tag{9}$$

where Tr() denotes the trace and * denotes the conjugate transpose. W^k is a diagonal weight matrix in the k-th iteration:

$$W_i^k = \frac{1}{\sqrt{\left(\nabla_x z_i^k\right)^2 + \left(\nabla_y z_i^k\right)^2}}, \text{ for } i = 1, 2, \ldots, N, \tag{10}$$

and

$$W^k = \begin{Bmatrix} W_1^k & & & \\ & W_2^k & & \\ & & \cdots & \\ & & & W_N^k \end{Bmatrix}. \tag{11}$$

A small constant $\mathscr{E}$ can be added to avoid W becoming infinity. It results in that $Q(z, W^k)$ is always greater or equal to $F(z)$ and is tangent to $F(z)$ at z^k:

$$Q\left(z, W^k\right) \ge F(z), \quad \forall z, \tag{12}$$

$$Q\left(z^k, W^k\right) = F\left(z^k\right). \tag{13}$$

Minimizing $F(z)$ directly would be difficult. Therefore we minimize its upper bound $Q(z, W^k)$ and update the weights W iteratively. This is the key idea of constructing efficient algorithm by MM framework [45] (also known as expectation maximization (EM) method). We iteratively update W^k with z^k and solve z^{k+1} based on current W^k. The method in Ref. [44] solves a special case of the problem, when $D_1 = D_2 = I$.

After the weight matrix is updated by (10) and (15), then the problem is to update z:

$$z^{k+1} = \arg\min_z Q\left(z, W^k\right). \tag{14}$$

This is a quadratic function and W^k is independent on z. Let $\partial Q(z, W^k)/\partial z = 0$ and we have:

$$\left(A^*A + \lambda D_1^* W^k D_1 + \lambda D_2^* W^k D_2\right) z = A^* y. \tag{15}$$

This step dominates the computational cost of the whole algorithm. If this subproblem cannot be solved efficiently, the total reconstruction speed will be slow. Obtaining the exact inverse of the system matrix $S = (A^*A + \lambda D_1^* W^k D_1 + \lambda D_2^* W^k D_2)$ in each iteration is usually intractable. An alternative way is to approximate the solution of (19) with the classical conjugate gradient (CG) decent method [40]. Besides CG, a better way is the preconditioned conjugate gradient (PCG) method [46], where a preconditioner should be predefined. The design of preconditioner P is problem-dependent, which should be as close as to the system

matrix S (accuracy) and the inverse P^{-1} can be acquired efficiently. Due to the tradeoff between the accuracy and efficiency, it is not an easy task.

A standard preconditioner is the diagonal Jacobi preconditioner, which directly removes all the non-diagonal elements of S [40]. Although the computational complexity is reduced significantly, such diagonal preconditioner is often not very accurate because all the non-diagonal information is lost. Can we find a more accurate preconditioner without increasing the computation complexity? As we will show soon, our preconditioner is non-diagonal and much more accurate, whose inverse can be obtained with the same computational complexity as the diagonal preconditioner. As a result, the overall convergence speed of the algorithm will be accelerated.

We observe that the matrix $R_t^* R_t$ is always diagonal, and more importantly, $A^*A = F^* R_t^* R_t F$ is therefore diagonally dominant. Note that this structure is independent to the data X. Thus, an accurate approximation could be made by removing the non-diagonal elements of A^*A. By the properties of the Fourier transform, all the diagonal elements of A^*A is equal to the mean of diagonal elements of R^*R, i.e. the sampling ratio s. Motivated by this, we define a new preconditioner $P = sI + \lambda D_1^* W^k D_1 + \lambda D_2^* W^k D_2$ to accelerate the whole algorithm, where I is the identity matrix. Due to the diagonally dominant structure of A^*A, this preconditioner is very accurate. Note that the Jacobi preconditioner removes the non-diagonal elements of $\lambda D_1^* W^k D_1 + \lambda D_2^* W^k D_2$, which is intuitively less accurate than ours.

Due to the structure of D_1 and D_2, the proposed preconditioner P is a penta-diagonal matrix and is symmetric, which has the following form:

$$P = \begin{bmatrix} a_1 & b_1 & & c_1 & & & \\ b_1 & a_2 & b_2 & & c_2 & & \\ & b_2 & a_3 & \cdots & & \cdots & \\ & & \cdots & \cdots & & & c_{N-n} \\ c_1 & & & & & & \\ & c_2 & & & & & \\ & & \cdots & & \cdots & \cdots & b_{N-1} \\ & & & c_{N-n} & & b_{N-1} & a_N \end{bmatrix} \tag{16}$$

There is no closed form for the inverse of P. Thanks to the diagonally dominant structure again; such penta-diagonal matrix has incomplete LU decomposition $P \approx LU$ where

$$L = \begin{bmatrix} 1 & & & & & & \\ \frac{b_1}{a_1} & 1 & & & & & \\ & \frac{b_2}{a_2} & 1 & & & & \\ & & \cdots & \cdots & & & \\ \frac{c_1}{a_1} & & & \frac{b_n}{a_n} & 1 & & \\ & \cdots & & & \cdots & \cdots & \\ & & \frac{c_{N-n}}{a_{N-n}} & \cdots & & \frac{b_{N-1}}{a_{N-1}} & 1 \end{bmatrix}, \tag{17}$$

$$U = \begin{bmatrix} a_1 & b_1 & \cdots & c_1 & & & \\ & a_2 & b_2 & \cdots & c_2 & & \\ & & \cdots & \cdots & & \cdots & \\ & & & a_{N-n} & b_{N-n} & \cdots & c_{N-n} \\ & & & & \cdots & \cdots & \\ & & & & & a_N & b_{N-1} \\ & & & & & & a_N \end{bmatrix}. \tag{18}$$

The decomposition is very accurate as P is diagonally dominated with $a_i \gg b_i^2$, $a_i \gg c_i^2$ and $a_i \gg b_i c_i$ for all i. Due to the sparse structure of P, the incomplete LU decomposition only takes linear time. Therefore, the total time to obtain $P^{-1} \approx U^{-1}L^{-1}$ is $\mathcal{O}(N)$. Now, we can conclude the proposed method in Algorithm 1. After z is solved, x_t can be obtained by $x_t = z + x_1$. To our best knowledge, this is the first study to accelerate MRI reconstruction with such preconditioner. We summarize the whole algorithm to solve (6) in Algorithm 1. All N-by-N matrices can be efficiently stored using sparse matrices in MATLAB.

Algorithm 1. dTV Reconstruction

Input: $A = R_t F$, x_1, $y = b_t - R_t F x_1$, z^1, λ, $k = 1$
Output: z, $x_t = z + x_1$.
while not meet the stopping criterion **do**
  Update W^k by (10)
  Update $S = A^*A + \lambda D_1^* W^k D_1 + \lambda D_2^* W^k D_2$
  Update $P = sI + \lambda D_1^* W^k D_1 + \lambda D_2^* W^k D_2 \approx LU$, $P^{-1} \approx U^{-1}L^{-1}$
  while not meet the PCG stopping criterion **do**
    Update z^{k+1} by PCG for $Sz = A^*y$ with preconditioner $P \approx LU$
  end while
  Update $k = k + 1$
end while

5. Results

5.1. Experiment setup

All experiments are conducted using MATLAB on a desktop computer with 3.4GHz Intel core i7 3770 CPU. We compare our method with two online method modified CS (MCS) [22],[1] the approach based on difference image (DI) [21] and two state-of-the-art offline methods k-t SLR [19][2] and the dictionary learning based method DLTG [13].[3] The latest codes are downloaded from each author's website and we use their default parameter settings for all experiments. For our method, we set $\lambda = 0.001$ for all experiments.

As MCS, DI, k-t SLR and DLTG are all designed for single channel imaging, the reconstruction of multi-channel data is not involved when comparing with them. In-vivo breath-held cardiac perfusion and cine datasets are used here [28,47].

The complex-valued data matrices are $192 \times 192 \times 40$ and $256 \times 256 \times 24$, which were combined by the original 12-channel data.

The proposed reconstruction method can be combined with the fast acquisition hardware radial FLASH [25] for real time imaging. Therefore, the radial sampling mask is used to simulate undersampling. The root-mean-square error (RMSE) is used as the metric for result evaluation. The sampling ratio is defined as the number of undersampled measurements divided by the number of full measurements. The ground-truth image is obtained by inverse FFT with full sampling.

In the final experiment, we compare our method with k-t SPARSE-SENSE on the original 12-channel cine datasets for parallel imaging. The original dataset was acquired with 4-fold acceleration by Cartesian sampling. We attach the demo code and the results with this submission.[4]

5.2. The effectiveness of the proposed method

As the proposed dTV is an extension to conventional spatial TV, we compare the performance of them here. 3D TV and temporal TV cannot be applied on online reconstruction. Therefore, they are not included in these comparisons. The first frame is often required to be reconstructed very accurately for all online methods [22,21]. Therefore, we use 1/2 sampling for the first frame and 1/6 sampling

[1] http://www.ece.iastate.edu/namrata/software.html.
[2] http://user.engineering.uiowa.edu/jcb/software/ktslr_matlab/Software.html.
[3] http://www.doc.ic.ac.uk/jc1006/Jose_Caballero_-_Software.html.
[4] https://dl.dropboxusercontent.com/u/58080329/codeandresults.zip.

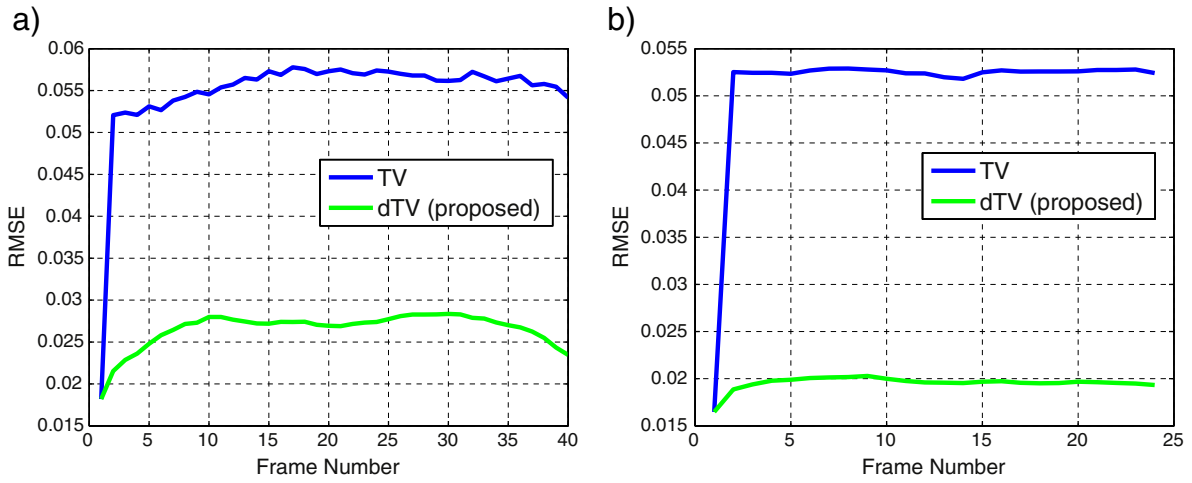

Fig. 3. Comparisons with conventional spatial TV and dTV. (a) On the perfusion dataset. (b) On the cine dataset.

for the rest frames. The results on the two datasets are presented in Fig. 3. We can observe that, the TV and dTV have the same results on the first frame, as there is no reference available. However, for the rest frames, the proposed method is significantly better. This is because the dTV exploits sparsity in both spatial and temporal domains, while conventional spatial TV can only utilize the spatial redundancy. When the sample ratio is reduced from 1/2 to 1/6, the results of TV become much worse. Due to image similarity in temporal direction, our method still can preserve high accuracy.

5.3. The efficiency of the proposed method

One of our contributions is the proposed preconditioner to accelerate MRI reconstruction. To validate the effectiveness of this preconditioner, we take experiments on the Shepp–Logan phantom image with 64×64 pixels, which is feasible to obtain the closed form solution of S^{-1} for evaluation. The Shepp–Logan phantom image is piece-wise smooth and an ideal example to validate TV/dTV reconstruction. We compare our method with Jacobi PCG and conjugate gradient (CG) method for the subproblem in each iteration. The relative errors for these methods compared with the closed form solution are shown in Fig. 4. The relative error is defined as $\|x - x^*\|_2/\|x^*\|_2$, where x^* is the optimal solution.

It shows that only 20 iterations of PCG with the proposed preconditioner can outperform conventional CG with 200 iterations. Note that the time complexities of each iteration in PCG and CG are the same. As expected, the overall computational time for each method is very close. Jacobi PCG requires approximately 2 times of iterations to reach the same accuracy of ours, which is because it discards all non-diagonal information directly and makes the preconditioning less precise. The later experiments show that only 10–30 iterations of the inner PCG loop are sufficient for accurate reconstruction.

5.4. Reconstruction accuracy comparisons

First, we use 1/2 sampling for the first frame and 1/6 sampling for the rest frames, the same as the above setting. The reconstruction RMSEs are shown in Fig. 5 on the two datasets. From the results, it is obvious that the previous online methods [22,21], have larger reconstruction errors than the offline methods [13,19] while the proposed method is comparable or even better than the k-t SLR [19] and DLTG [14] on both datasets in terms of RMSE. DI does not perform as good as that presented in the paper [21]. From the 4th and 5th frame, it starts to fail. However, in Ref. [21], the curve of DI is often between those of k-t SLR and MCS. We found that it used the full sampling for the first frame, while the reconstruction error occurs at the first frame here with 1/2 sampling. With the same setting in

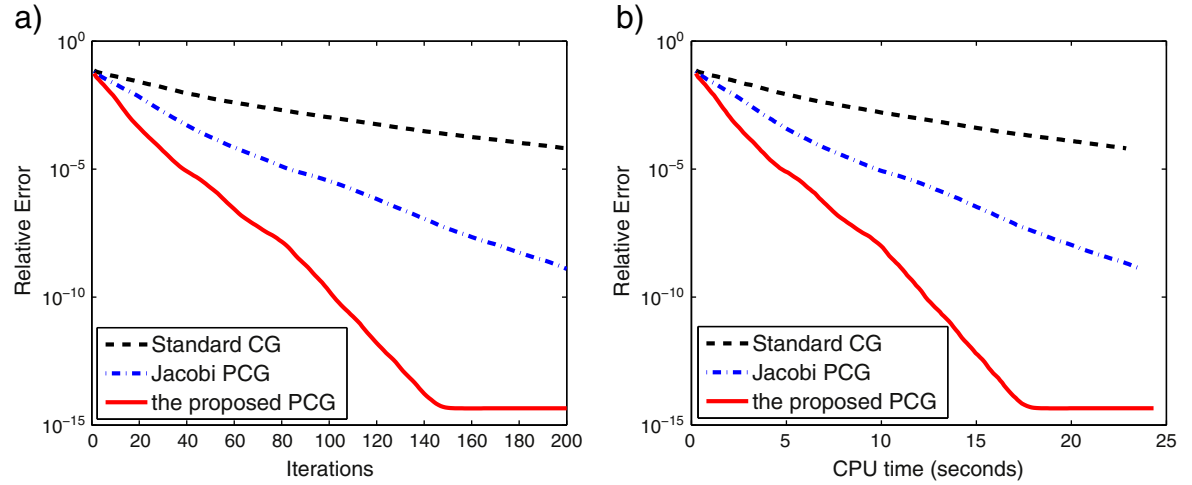

Fig. 4. Reconstruction error comparison among CG, Jacobi PCG and the proposed PCG on the Shepp–Logan phantom image. (a) Reconstruction error to the number of iterations. (b) Reconstruction error to the executional time.

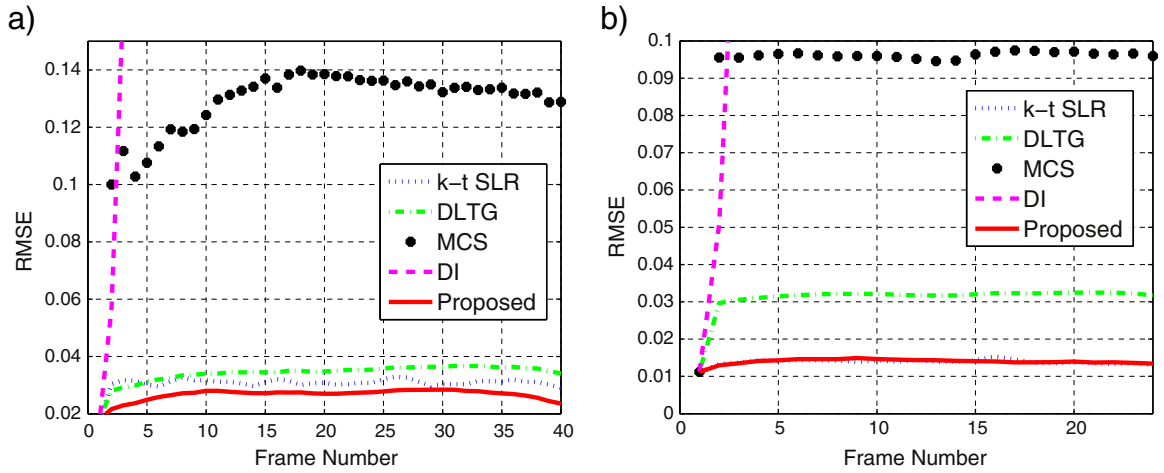

Fig. 5. Reconstruction accuracy comparisons of different methods. (a) On the perfusion dataset. (b) On the cine dataset. Our method and k-t SLR almost overlap on the second dataset.

Ref. [21], we conduct additional experiments for DI. It shows that DI starts to fail after 20–30 frames. These results demonstrate that DI is very sensitive to error accumulation.

The third frames of the results are presented in Figs. 6 and 7 for the two datasets, respectively. k-t SLR [19], DLTG [14] and our method provide high quality images, while visible artifacts can be obviously observed on the images reconstructed by MCS and DI. From the RMSE and the visual comparisons, our online method is quite comparable to the state-of-the-art offline methods, if not better. The superiority of our method over the previous online methods [21,22], is

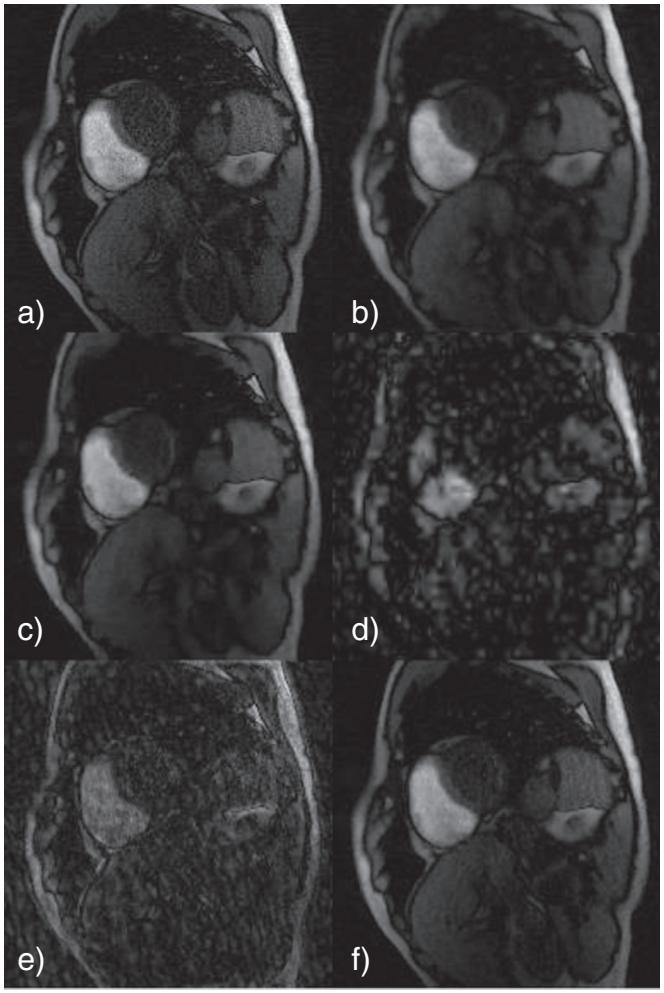

Fig. 6. Results of the third frame of the perfusion sequence at sampling ratio 1/6. (a) The image with full sampling. The rest images are reconstructed by (b) k-t SLR; (c) DLTG; (d) MCS; (e) DI; (f) the proposed method.

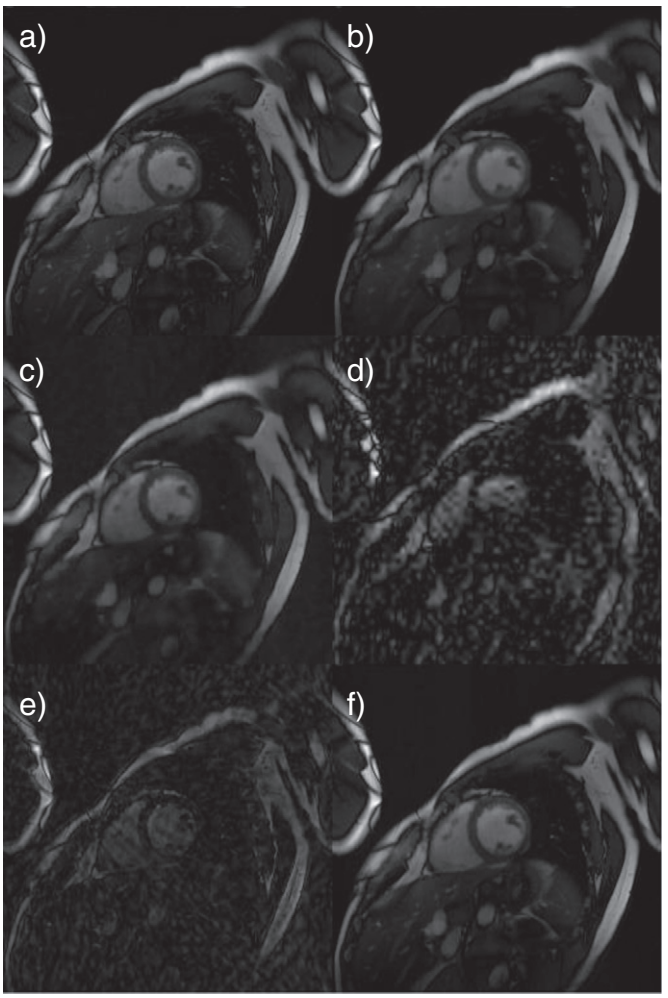

Fig. 7. Results of the third frame of the cine sequence at sampling ratio 1/6. (a) The image with full sampling. The rest images are reconstructed by (b) k-t SLR; (c) DLTG; (d) MCS; (e) DI; (f) the proposed method.

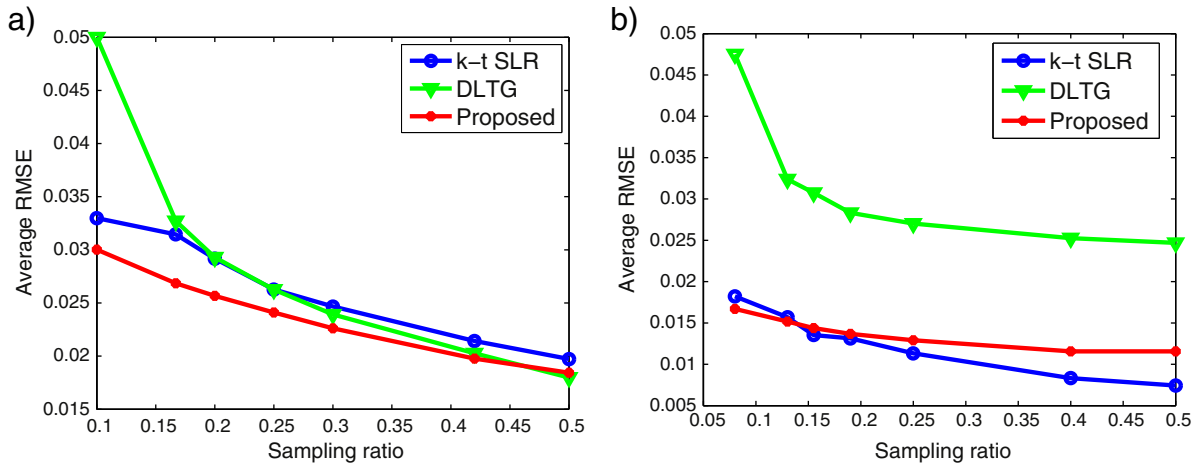

Fig. 8. Comparisons with the offline methods k-t SLR and DLTG at different sampling ratios. (a) On the perfusion dataset. (b) On the cine dataset.

very clear. Therefore, we do not compare their error images and zoomed-in areas in details.

We vary the sampling ratios of the second frame to the end frame and compare their average reconstruction errors. These experimental results are presented in Fig. 8, which demonstrates the comparable performance of our method to the state-of-the-art offline methods. At a low sampling ratio that we are interested, the proposed method seems to be even better than k-t SLR and DLTG. From the results on both datasets, it shows that DLTG are not stable at low sampling ratios. As the previous online methods [22,21], are much less accurate, they are not compared in these experiments.

Since our method requires the first frame (reference image) to be accurate, we evaluate its sensitivity to the accuracy of the first frame. Keep 1/6 sampling ratio for the second frame to the end frame, we vary the sampling ratio of the first frame. Fig. 9 shows the RMSEs of the results when the sampling ratios of the first frames are 100%, 75%, 50% and 25%.

It can be clearly observed that the accuracies of the first frames vary significantly, due to the different sampling ratios. For the rest frames, the reconstruction errors are very close, when the first frame is reconstructed with 100%, 75% or 50%. It is slightly worse for the case with 25%, while this result is still comparable to the results of k-t SLR and DLTG in Fig. 5(a). It demonstrates that our method is not sensitive to the accuracy of the first frame. There is an interesting point in Fig. 9. The second frame recovered from 1/6 sampling even is more accurate than the first frame with 25% sampling. It is because the first frame is reconstructed without a reference image to guide the reconstruction. This further confirms the advantages of the dTV to exploit temporal and spatial redundancies.

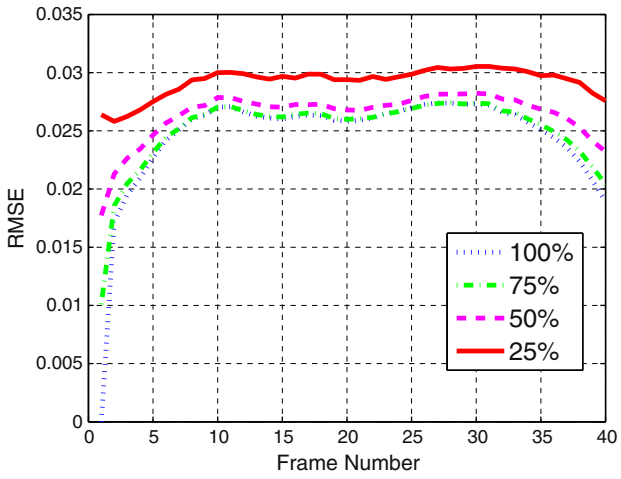

Fig. 9. The reconstruction RMSEs of different sampling ratios of the first frame on the perfusion dataset by the proposed method. The rest frames always are reconstructed with 1/6 sampling.

5.5. Reconstruction speeds

We list the total reconstruction times of all the methods in Table 2, which correspond to the experiments in Fig. 5. SVD decomposition is involved in k-t SLR, which makes it not scalable. When the image size increases from 192 × 192 to 256 × 256, the reconstruction time almost increases 8 times. In each iteration of DLTG, the dictionary is re-trained. It costs more than an hour on each dataset. MCS [22] is very slow, as it is required to detect the support set of the wavelet coefficients in every iteration. The average reconstruction speeds for DI [21] and our method are 0.25 s/frame and 0.71 s/frame, respectively. Compared with DI [21], our method can achieve significant better results, especially when the first frame is not reconstructed exactly accurately. The current speed of our method is for the MATLAB implementation. The speed can be further improved with more efficient implementation (e.g. C++, GPU).

Our system is not the same as those in existing online methods [22,21]. After the reference image is available, the reconstructed speed can be as fast as the data acquisition speed. There is no need to wait for the previous reconstruction. Let T_a be the acquisition time and T_{re} be the reconstruction time of each frame. Supposing $T_{re} >> T_a$ as discussed above, previous online methods approximately cost $\mathcal{O}(T_{re})$ while the imaging time for our method can be $\mathcal{O}(T_a)$ when it is implemented in parallel. Therefore, the proposed method is significantly faster when the number of frames is large.

Table 2
The reconstruction times (seconds) of different methods on the two datasets.

	Perfusion (192 × 192 × 40)	Cine (256 × 256 × 24)
k-t SLR [19]	268.8	2119.5
DLTG [13]	5725.6	5803.3
MCS [22]	36903	36706
DI [21]	15.2	10.1
Proposed	28.4	33.1

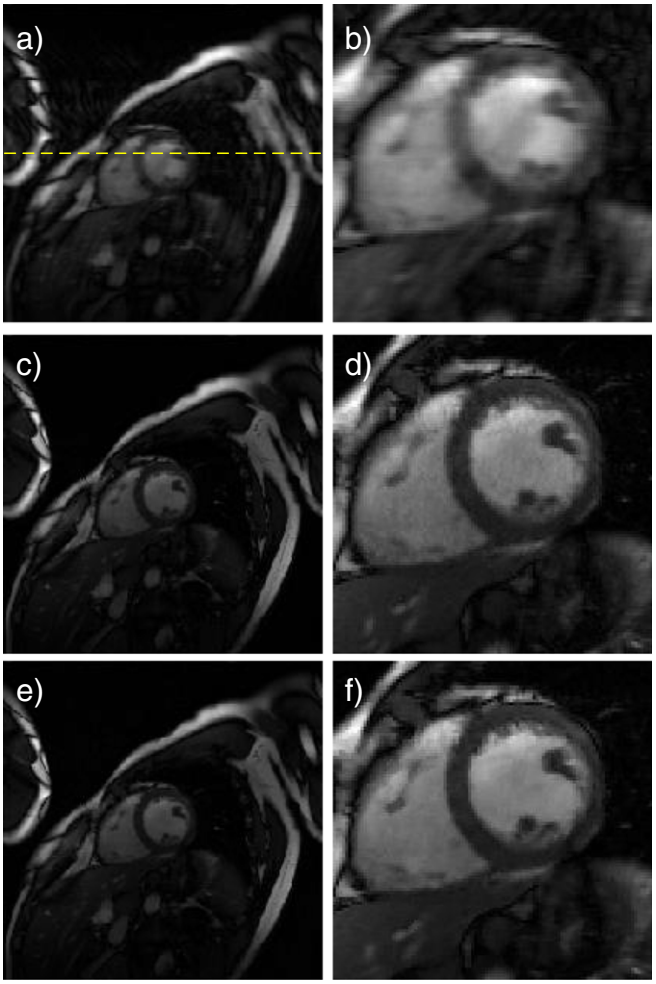

Fig. 10. The reconstructed third frames from the original cardiac cine datasets by (a) zero-filled FFT, (c) k-t SPARSE-SENSE, (e) dTV with their zoomed in areas of interest (b)(d)(f), respectively.

5.6. Parallel Imaging

Finally, we compare our method with k-t SPARSE-SENSE [28] for parallel imaging. The original cine dataset in Ref. [47] is used here, which was acquired with 25% sampling ratio for all frames.

As the coil sensitivities of this dataset were known, we use the extended version (4) for reconstruction.

Fig. 10 presents the reconstruction results from the measurements of 12 receiver coils. It shows that both k-t SPARSE-SENSE and our method provide high quality images, while the image by zero-filled FFT is noisy and blurry. If we take a close look at the zoomed-in area of interest, the result by our method seems even less noisy than that by k-t SPARSE-SENSE. This is because the temporal FFT used in k-t SPARSE-SENSE cannot exploit the spatial sparsity. However, the dTV can utilize the sparsity in both spatial and temporal domains. It encourages the image to be piece-wise smooth, and the image is automatically denoised when reconstruction. The temporal cross sections shown in Fig. 10 further confirm such observations. It is worthwhile to note that k-t SPARSE-SENSE cannot be used for online reconstruction. (See Fig. 11.)

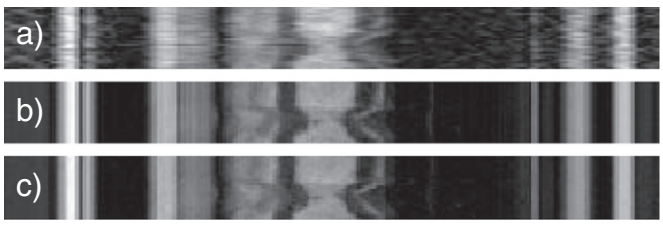

Fig. 11. Temporal cross sections indicated by the yellow dashed line in Fig. 10. (a) Zero-filled FFT. (b) k-t SPARSE-SENSE. (c) dTV.

6. Conclusion

In this paper, we have proposed a parallel reconstruction scheme for dMRI, a robust model to exploit both spatial and temporal redundancies, and an accelerated reweighted least squares algorithm to solve the reconstruction problem. Our motivation is that the first frame (reference image) can provide valuable information to guide the later reconstructions. A pre-scanned image can also be used as the reference image in this scheme. The proposed method can be easily combined into the parallel imaging technique with multiple receiver coils. Experiments on *in-vivo* cardiac perfusion and cine datasets have validated the efficiency and effectiveness of our method over the state-of-the-art methods. These contributions make real time dMRI much more feasible than before.

References

[1] Donoho D. Compressed sensing. IEEE Trans Inf Theory 2006;52(4):1289–306.
[2] Candès E, Romberg J, Tao T. Robust uncertainty principles: exact signal reconstruction from highly incomplete frequency information. IEEE Trans Inf Theory 2006;52(2):489–509.
[3] Lustig M, Donoho D, Pauly J. Sparse MRI: the application of compressed sensing for rapid MR imaging. Magn Reson Med 2007;58(6):1182–95.
[4] Lustig M, Santos JM, Donoho DL, Pauly JM. k-t SPARSE: high frame rate dynamic MRI exploiting spatio-temporal sparsity. Proc. the Annual Meeting of ISMRM; 2006. p. 2420.
[5] Gamper U, Boesiger P, Kozerke S. Compressed sensing in dynamic MRI. Magn Reson Med 2008;59(2):365–73.
[6] Huang J, Zhang S, Metaxas D. Efficient MR image reconstruction for compressed MR imaging. Med Image Anal 2011;15(5):670–9.
[7] Huang J, Chen C, Axel L. Fast multi-contrast MRI reconstruction. Proc. Int. Conf. MICCAI; 2012.
[8] Chen C, Huang J. The benefit of tree sparsity in accelerated MRI. Med Image Anal 2014;18(6):834–42.
[9] Berman BP, Mandava S, Bilgin A. On compressed sensing reconstruction for magnetic resonance imaging. Computer Vision in Medical Imaging. World Scientific Publishing; 2013.
[10] Gupta V, Van de Giessen M, Kirisli H, Kirschbaum SW, Niessen WJ, Lelieveldt B. Robust motion correction in the frequency domain of cardiac MR stress perfusion sequences. Proc. Int. Conf. MICCAIHeidelberg: Springer; 2012. p. 667–74.
[11] Xue H, Guehring J, Srinivasan L, Zuehlsdorff S, Saddi K, Chefdhotel C, et al. Evaluation of rigid and non-rigid motion compensation of cardiac perfusion MRI. Proc. Int. Conf. MICCAIHeidelberg: Springer; 2008. p. 35–43.
[12] Jung H, Sung K, Nayak KS, Kim EY, Ye JC. k-t FOCUSS: a general compressed sensing framework for high resolution dynamic MRI. Magn Reson Med 2009; 61(1):103–16.
[13] Caballero J, Rueckert D, Hajnal JV. Dictionary learning and time sparsity in dynamic MRI. Proc. Int. Conf. MICCAIHeidelberg: Springer; 2012. p. 256–63.
[14] Caballero J, Price A, Rueckert D, Hajnal J. Dictionary learning and time sparsity for dynamic MR data reconstruction. IEEE Trans Med Imaging 2014;33(4):979.
[15] Wang Y, Ying L. Accelerating dynamic MRI using patch-based spatiotemporal dictionaries. Proc. the Annual Meeting of ISMRM; 2013. p. 3446.
[16] Ravishankar S, Bresler Y. MR image reconstruction from highly undersampled k-space data by dictionary learning. IEEE Trans Med Imaging 2011;30(5):1028–41.
[17] Usman M, Prieto C, Schaeffter T, Batchelor P. k-t group sparse: a method for accelerating dynamic MRI. Magn Reson Med 2011;66(4):1163–76.
[18] Prieto C, Usman M, Wild J, Kozerke S, Batchelor P, Schaeffter T. Group sparse reconstruction using intensity-based clustering. Magn Reson Med 2013;69(4): 1169–79.
[19] Lingala SG, Hu Y, DiBella E, Jacob M. Accelerated dynamic MRI exploiting sparsity and low-rank structure: k-t SLR. IEEE Trans Med Imaging 2011;30(5):1042–54.
[20] Sümbül U, Santos JM, Pauly JM. A practical acceleration algorithm for real-time imaging. IEEE Trans Med Imaging 2009;28(12):2042–51.
[21] Majumdar A, Ward R, Aboulnasr T. Compressed sensing based real-time dynamic MRI reconstruction. IEEE Trans Med Imaging 2012;31(12):2253–66.
[22] Vaswani N, Lu W. Modified-CS: modifying compressive sensing for problems with partially known support. IEEE Trans Signal Process 2010;58(9):4595–607.

[23] Liang D, DiBella EV, Chen R-R, Ying L. k-t ISD: dynamic cardiac MR imaging using compressed sensing with iterative support detection. Magn Reson Med 2012; 68(1):41–53.
[24] Ji J, Lang T. Dynamic MRI with compressed sensing imaging using temporal correlations. IEEE Int. Symp. Biomed. Imag; 2008. p. 1613–6.
[25] Zhang S, Block KT, Frahm J. Magnetic resonance imaging in real time: advances using radial FLASH. J Magn Reson Imaging 2010;31(1):101–9.
[26] Uecker M, Zhang S, Voit D, Karaus A, Merboldt K-D, Frahm J. Real-time MRI at a resolution of 20 ms. NMR Biomed 2010;23(8):986–94.
[27] Chen C, Li Y, Axel L, Huang J. Real time dynamic MRI with dynamic total variation. Proc. Int. Conf. MICCAI; 2014.
[28] Otazo R, Kim D, Axel L, Sodickson DK. Combination of compressed sensing and parallel imaging for highly accelerated first-pass cardiac perfusion MRI. Magn Reson Med 2010;64(3):767–76.
[29] Zhao B, Haldar JP, Brinegar C, Liang Z-P. Low rank matrix recovery for real-time cardiac MRI. IEEE Int. Symp. Biomed. Imag; 2010. p. 996–9.
[30] Chen L, Schabel MC, DiBella EV. Reconstruction of dynamic contrast enhanced magnetic resonance imaging of the breast with temporal constraints. Magn Reson Imaging 2010;28(5):637–45.
[31] Montefusco LB, Lazzaro D, Papi S, Guerrini C. A fast compressed sensing approach to 3D MR image reconstruction. IEEE Trans Med Imaging 2011;30(5):1064–75.
[32] Lang T, Ji J. Accelerating dynamic contrast-enhanced MRI using compressed sensing. Proc. the Annual Meeting of ISMRM; 2008. p. 1481.
[33] Fischer A, Breuer F, Blaimer M, Seiberlich N, Jakob P. Accelerated dynamic imaging by reconstructing sparse differences using compressed sensing. Proc. the Annual Meeting of ISMRM; 2008. p. 3–9.
[34] Sumbul U, Santos JM, Pauly JM. Improved time series reconstruction for dynamic magnetic resonance imaging. IEEE Trans Med Imaging 2009;28(7):1093–104.
[35] Asif MS, Hamilton L, Brummer M, Romberg J. Motion-adaptive spatio-temporal regularization for accelerated dynamic MRI. Magn Reson Med 2013;70(3): 800–12.
[36] Tsao J, Kozerke S. MRI temporal acceleration techniques. J Magn Reson Imaging 2012;36(3):543–60.
[37] Chen G-H, Tang J, Leng S. Prior image constrained compressed sensing (piccs): a method to accurately reconstruct dynamic ct images from highly undersampled projection data sets. Med Phys 2008;35(2):660–3.
[38] Pruessmann KP, Weiger M, Scheidegger MB, Boesiger P, et al. SENSE: sensitivity encoding for fast MRI. Magn Reson Med 1999;42(5):952–62.
[39] Chen C, Li Y, Huang J. Calibrationless parallel MRI with joint total variation regularization. Proc. Int. Conf. MICCAIHeidelberg: Springer; 2013. p. 106–14.
[40] Rodrguez P, Wohlberg B. Efficient minimization method for a generalized total variation functional. IEEE Trans Image Process 2009;18(2):322–32.
[41] Huang J, Zhang S, Li H, Metaxas D. Composite splitting algorithms for convex optimization. Comput Vis Image Und 2011;115(12):1610–22.
[42] Ramani S, Fessler JA. Parallel MR image reconstruction using augmented Lagrangian methods. IEEE Trans Med Imaging 2011;30(3):694–706.
[43] Chen C, Huang J, He L, Li H. Preconditioning for accelerated iteratively reweighted least squares in structured sparsity reconstruction. Proc. IEEE Conf. Computer Vision and Pattern Recognition; 2014. p. 2713–20.
[44] Daubechies I, DeVore R, Fornasier M, Güntürk CS. Iteratively reweighted least squares minimization for sparse recovery. Commun Pure Appl Math 2010;63(1):1–38.
[45] Hunter DR, Lange K. A tutorial on MM algorithms. Am Stat 2004;58(1):30–7.
[46] Saad Y. Iterative methods for sparse linear systems. SIAM; 2003.
[47] Otazo R, Feng L, Chandarana H, Block T, Axel L, Sodickson DK. Combination of compressed sensing and parallel imaging for highly-accelerated dynamic MRI. IEEE Int. Symp. Biomed. Imag.; 2012. p. 980–3.